Effects of Deoxidation Practice on the Inclusion Formation in Low Alloy Structural Steels

Casper van der Eijk, Øystein Grong, and John Walmsley

Casper van der Eijk and John Walmsley are researchers at
SINTEF Materials Technology
N-7465 Trondheim, Norway.
Fax: +47-73597043
Tel: +47-73596857

Øystein Grong is professor at the
Norwegian University of Science and Technology
Department of Materials Technology and Electrochemistry
N-7491 Trondheim, Norway.

Key Words: steel, inclusions, deoxidation

Abstract

In the present investigation, the sequence of inclusion formation in two Ti-deoxidised steels and one Al-Ca deoxidised steel have been examined by means of electron microscopy in combination with a thermodynamic analysis of the phase relations involved. It is concluded that the Ti-containing inclusions form as a result of a series of reactions occurring in the ladle, during solidification and in the solid state. In contrast, the primary inclusions in the Al-Ca deoxidised steel are complex oxysulphides, which are thermodynamically more stable and therefore form in the liquid state. The implications of these findings for choice of steel deoxidation practice are briefly discussed.

INTRODUCTION

Inclusions commonly found in steels are either exogenous or indigenous, depending on their origin.[1] The first type arises from entrapment of slag or oxide particles rejected by the lining, while the second type forms within the system as a result of deoxidation reactions (oxides) or precipitation reactions (nitrides, sulphides). Depending on the applied alloying and deoxidation practice, a variety of indigenous inclusions may form.[2,3] These range from pure oxides and sulphides to complex multiphase particles that resemble those commonly found in steel weld metals.[4-10] The latter group is known be heterogeneous in nature both with respect to chemistry, shape, and crystallographic properties, and forms as a result of a series of nucleation events taking place during cooling, both in the liquid and in the solid state .[11-13]

Over the past decades, significant improvement of steel properties has been achieved through strict control of the chemical composition, volume fraction and size distribution of non-metallic inclusions.[3] This has been made possible by the introduction of secondary steelmaking as an integrated step in the production route and the use of advanced ladle refining techniques for deoxidation and desulphurisation.[14,15] The detrimental effect of inclusions on steel properties arises from their ability to act as initiation sites for microvoids and cleavage cracks during service.[16,17] Hence, the use of clean steels is normally considered to be an advantage both from a toughness and a fatigue point of view.

More recently, the beneficial effect of inclusions on the steel transformation behaviour has been highlighted and recognised.[18] In particular, the phenomenon of intragranular nucleation of acicular ferrite at inclusions is well-documented in low alloy steel weld metals, where the best properties are achieved at elevated oxygen and sulphur levels owing to the development of a more fine-grained microstructure.[19,20] The same observations have also been made in wrought steel products,[4-7] although the conditions existing in steelmaking are more challenging due to the risk of inclusion coarsening and entrapment of large particles that can

act as initiation sites for cleavage cracks.[8] This makes it difficult to fully utilise the concept of inclusion-stimulated ferrite nucleation in structural steels through excessive oxygen and sulphur additions without compromising toughness.

Partly because of the problems related to control of the impurity level in full-scale production, only a limited number of steels containing interactive oxide particles are currently available on the commercial marked. However, the results obtained so far on titanium deoxidised steels are encouraging and clearly demonstrate the potential of utilising the concept of intragranular nucleation of ferrite at inclusions as a means to improve the heat affected zone (HAZ) toughness during high heat input welding.[4,8] This situation calls for a closer examination of the mechanisms of inclusion formation in titanium-deoxidised steels, based on optical and electron microscopy in combination with a more in-depth thermodynamic analysis of the phase relations involved.

EXPERIMENTS

The experimental programme includes a full metallographic characterisation of inclusions which form in low carbon microalloyed steels under different deoxidation conditions.

Materials

Three steels, in the following designated steels A, B and C, were obtained from a German steel manufacturer (Dillinger Hüttenwerke). These steels are continuously cast and were received in the form of rectangular slabs with a thickness of 288 mm. Steels A and B are deoxidised using Ti, while C is a reference steel which is deoxidised using Al-Ca. Their chemical compositions are summarised in Table I.

Scanning Electron Microscopy

The Energy Dispersive X-ray Spectroscopy (EDS) inclusion analyses were done with full ZAF corrections, using a Jeol™ 840 scanning electron microscope. A minimum of 20 inclusions were examined in each slab positions using an acceleration voltage of 20 kV. In these measurements a relatively large spot size

of the incident electron beam was employed to determine the average composition of the inclusions. Iron was subsequently excluded from the element population to eliminate the contribution of stray signals from the steel matrix. The content of the remaining elements were then normalised to 100% and reported as weight percent (arbitrary units).

Transmission Electron Microscopy

The Transmission Electron Microscopy and Scanning Transmission Electron Microscopy (TEM/STEM) inclusion analyses were carried out using a Philips CM 30 transmission electron microscope equipped with an EDS unit for element analyses. A special preparation technique was employed to achieve transparent foils with the inclusions embedded in the steel matrix. This technique utilises initial electropolishing to perforate the foil in combination with ion-beam thinning of the inclusions.

By means of this thin foil technique, the composition of the inclusion constituent phases has been documented by EDS analyses and X-ray imaging. The crystal structure and orientation of the phases have been determined by Selected Area Electron Diffraction (SAD).

RESULTS

In the following, the main results from the inclusion analyses will be presented in order to reveal details of their chemical composition and crystal structure, as influenced by applied deoxidation practice.

Constituent elements and phases in the inclusions

The results from the EDS analyses of the complex oxysulphide inclusions are summarised in Table II. The large spread in the chemical composition observed for these inclusions indicates that they are of a heterogeneous chemical nature. Nevertheless, the data reveal a clear effect of the applied deoxidation practice on the resulting inclusion chemistry. Considering steels A and B, the inclusions are

seen to be rich in Ti, Mn, and S. In contrast, in the reference steel C; Al, Ca, Mn, and S are the main constituent elements entering the inclusions.

Figure 1 shows the element distribution and constituent phases in an oxysulphide inclusion from steel A. According to these STEM-EDX maps, both Al, Ti, and Mn are present within the oxide core. But a rod-shaped Al rich phase is present which does not mix with the Ti-Mn rich phase. Moreover, Mn and S are located on the surface, presumably in the form of MnS. In addition, TiN is present at the surface. These results are consistent with those reported by others.[4,6,7,9]

Figure 2 shows the same inclusion as in Figure 1. The arrow in Figure 2 indicates where the linescan is taken across the inclusion. Figure 3a shows the result of this linescan and Figure 3b the ratio between the Ti and the Mn counts. It is clear that this ratio is not constant in all positions across the Ti-oxide. Hence, the Ti-rich regions do not appear to have the same composition. In particular, the high Ti peak observed at the interface between the Ti-Mn-oxide and the Fe matrix indicates the presence of TiN on the surface of the inclusion.

Attempts were also made to identify the different constituent phases by means of diffraction pattern analyses. Three different oxide phases are indicated in Figure 4. Two are identified as rhombohedral $MnOTiO_2$ (phase No. 1) and hexagonal Al_2O_3CaO (phase No. 2), respectively. The crystal structure of phase No. 3, which corresponds to the more pure Ti-oxide phase facing the MnS, could not be identified with certainty. The surface phase (No. 4) was identified by diffraction analyses as α-MnS. The angular morphology of the MnS layer is characteristic for MnS precipitated in the solid state.[21] Presumably a layer of TiN is present at the surface (indicated as No. 5), but this could not be identified as such by means of diffraction pattern analyses.

DISCUSSION

Inclusion formation takes place at various stages of the steelmaking process, e.g. in the ladle, during solidification and in the solid state. However, since only the end product of the different processes is known and can be observed in the

microscope, a retrospective glance on the contribution from the previous process steps to the crystalline heterogeneity of the inclusions is required.

Predictions of phase relations

In order to unravel the sequence of inclusion formation both prior to, during and after solidification, detailed thermodynamic analyses have been carried out using Thermo-Calc.[22,23] In the present investigation, the Irsid, sub94 and ssol databases are used to obtain the required information about the thermodynamic stability of the different inclusion constituent phases at various stages of the steelmaking process. Three different calculation methods were adopted:

(i) General Al/Ti deoxidation diagrams. In industrial steelmaking practice, it will be almost impossible to produce steel which does not contain minor amount of Al. Therefore the expected deoxidation products in the case of deoxidation with a combination of Al and Ti are calculated.

(ii) The global equilibrium approach, where full thermodynamic equilibrium is assumed at each temperature. This method is used to calculate the stability of different phases before and during solidification. Whether full equilibrium, in reality, is maintained down to the solidus temperature depends on the kinetics, but rate phenomena and element partitioning during solidification are not considered in the analysis.

(iii) The local equilibrium approach, where equilibrium is restricted to a small volume of steel enclosing the inclusions. These calculations are used to examine possible changes in the inclusion chemistry due to reactions occurring in the solid state.

Figure 5 shows the expected deoxidation products at 1800K in the case where Ti deoxidation takes place in the presence of small amounts of Al. The diagram is calculated for a steel containing 0.003wt% O and 0.06wt% C. The diagram shows clearly the large difference in affinity to oxygen between Al and Ti.

The predicted sequence of inclusion formation in the three steels with decreasing temperature is shown in Figure 6. In the case of steel A, only Al_2O_3CaO is stable prior to solidification. During solidification Ti-oxides become stable, first in the form of Ti_3O_5 and later as Ti_2O_3. MnS becomes a stable phase right after solidification. Hence, precipitation is likely to take place in the solid state. This, in turn, may explain why the MnS tends to have a faceted morphology, as shown previously in Figure 4. Steel B behaves in a slightly different manner in that the primary Al_2O_3CaO phase becomes unstable during solidification and is later replaced by Ti_2O_3. This is due to the higher Ti content and the lower O content in steel B compared with steel A.

In contrast, the predicted sequence of oxide formation in the Al-Ca deoxidised steel C is quite different from that observed in the Ti deoxidised steels. According to Thermo-Calc, only different Al-Ca-O compounds and sulphides are expected to form under the prevailing circumstances. However, during the final stage of solidification TiN starts to precipitate because Ti is not bound as oxides in this particular steel.

Conditions for MnS formation

The fact that the inclusions contain an appreciable amount of MnS is better illustrated in Figure 7, which shows plots of the Mn content versus the S content in the inclusions present in steels A and B. The strong correlation between the S and Mn levels suggests that the large scatter observed in the SEM-EDS analyses (see Table II) simply reflects natural fluctuations in the MnS content between the inclusions. Moreover, a closer examination of Figure 7 reveals that the slope of the trendlines does not depart significantly from 1.7, which is the stoichiometric Mn to S ratio in pure MnS. It follows that the remaining Mn, which is not bound as MnS, will be present in the Ti-rich part of the oxide core as indicated in Figure 7.

Global equilibrium vs. local equilibrium

Assessment of the departure from global equilibrium down to the solidus temperature can be done on the basis of the Thermo-Calc data contained in Figure 6 and the SEM-EDS inclusion data summarised in Table II. The results are shown in Table III. The calculated values refer to the results right after solidification (1760K). Note that the predicted compositions are based on the assumption that all phases are present within the same inclusion and not as separate particles in the steel matrix.

Considering the Al-Ca deoxidised steel C, the analysed and calculated inclusion compositions are in fair agreement with each other, except for the Mg and Ti contents. Mg is an impurity element coming from the lining and is therefore not accounted for in the calculations. In addition, Thermo-Calc predicts that TiN should start to form during the later stages of the solidification process, leading to a Ti content which is appreciably higher than that observed experimentally. This discrepancy does not necessarily imply a departure from global equilibrium, but suggests that the TiN precipitates are present as separate particles in the steel matrix rather than at the surface of the oxysulphides. The latter interpretation is supported by the observation of pure TiN particles in the lightmicroscope, which means that the assumption of global equilibrium down to the solidus temperature is a fair one under the prevailing circumstances. Hence, the good agreement obtained between calculated and analysed S contents confirms that the primary inclusions in steel C are complex Al-Ca oxysulphides.

Referring to Table III, a much larger discrepancy between measured and predicted inclusion compositions is observed for the two Ti-deoxidised steels. This is because MnS will partly precipitate as isolated particles in the interdendritic regions and partly at the surface of the oxides (Figure 7). A correction for the presence of MnS at the surface of the oxides can be done via the sulphur analyses, from which the pure oxide core composition can be estimated and compared with the corresponding Thermo-Calc predictions. The results are summarised in Table IV. Even after this correction, the discrepancy between the measured and predicted oxide core compositions is striking, particularly when it comes to Ti and

Mn. However, the origin of the observed discrepancy should be quite obvious when it is realised that TiN may be present in various amounts on the surface of the inclusions at the same time as the oxide core contains significant amounts of Mn (Figure 7). Since a thermodynamic consideration of the phase relations involved does not reveal any indication of these elements down to the solidus temperature, it is reasonable to assume that the final inclusion composition in the Ti-deoxidised steels is also affected by reactions occurring in the solid state.

Solid state reactions

The formation of TiN on the inclusions will take place in the solid state. Since most of the Ti is consumed in oxide formation, the amount of free Ti available for TiN-formation is limited.

However, the TiN formation on the surface of the oxides is possible if Ti is extracted from the core. Thermo-Calc predictions carried out on a closed system[24], show that replacement of Ti by Mn is thermodynamically favourable and will lead to formation of TiN on the surface of the inclusions. Thus, the TiN formation can be represented by the following exchange reaction:

$$Ti_2O_3 + Mn + N \rightarrow MnOTiO_2 + TiN \qquad (1)$$

The $MnOTiO_2$ phase was found to be present in the inclusion shown in Figure 4, and is located next to the phase that is thought to be TiN. At the same time the more pure Ti-oxide is located adjacent to the MnS. These observations are consistent with the Thermo-Calc predictions.

The sequence of inclusion formation in Ti-deoxidised steels

Referring to Figure 8, the sequence of inclusion formation in Ti-deoxidised steels can be summarised as follows. Prior to solidification, strong deoxidisers like Al and Ca react with dissolved oxygen in the liquid steel to form the core of inclusions on which the Ti-oxides grow epitaxially during solidification. During the final stage of solidification some MnS precipitation occurs in the interdendritic

regions due to element partitioning. The remaining S precipitates on the oxides as MnS in the solid state. At even lower temperatures TiN becomes a stable phase. Provided that free Ti is present in the matrix, pure TiN may nucleate and grow directly in the austenite, as observed in steel B. Conversely, if most of the Ti already is tied-up in the oxide core as in steel A, the TiN formation occurs probably through an exchange reaction with Ti_2O_3. This gives $MnOTiO_2$ as a secondary reaction product, with Mn being absorbed from the adjacent steel matrix. The manganese compound formation at the surface of the inclusions is consistent with the observation of a Mn depleted zone in their vicinity.

SUMMARY

The conclusions that can be drawn from this investigation are the following:

- The SEM-EDS analysis shows a clear effect of the applied deoxidation practice on the resulting inclusion chemistry. Considering the Al-Ca killed steel C; Al, Ca, and S along with oxygen are the main constituent elements entering the inclusions. In contrast, the inclusions in the two titanium-deoxidised steels A and B are rich in Ti, Mn and S.
- The subsequent TEM/STEM examination shows that the inclusions in the two Ti-deoxidised steels are of a heterogeneous crystalline nature. Three different constituent phases have been identified by means of selected area diffraction pattern analyses, i.e. $MnOTiO_2$, Al_2O_3CaO and α-MnS. In addition, the indications are that both Ti_2O_3 and TiN are present in the inclusions.
- Based on a thermodynamic consideration of the phase relations involved, it can be argued that neither $MnOTiO_2$, α–MnS nor TiN will form under equilibrium conditions down to the solidus temperature. However, if the analysis is restricted to a small volume of steel surrounding the inclusions, these phases become thermodynamically stable in the solid state.
- In contrast, the primary inclusions in the reference steel C are complex oxysulphides. These are thermodynamically stable in liquid steel, and will therefore form during the early stages of the deoxidation process without undergoing compositional changes in the solid state.

ACKNOWLEDGEMENTS

The authors acknowledge the financial support provided by Elkem, Tinfos Jernverk, Fesil and the Norwegian Research Council through The Norwegian Ferroalloy Research Organisation (FFF).

REFERENCES

1. E.T. Turkdogan, Fundamentals of Steelmaking;, The Institute of Materials, London, 1996.
2. R. Kiessling and N.Lange, Non-Metallic Inclusions in Steel, The Metals Society (TMS), London, 1978.
3. A. Nicholsen and T. Gladman, Ironmaking and Steelmaking, vol.13, (2), 1986, p.53.
4. K. Yamamoto, S. Matsuda, T. Haze, R, Chijiiwa and H. Mimura, Proc. Int. Symp. "Residual and Unspecified Elements in Steel". Bal Harbour Fl (USA), 11-13 Nov. 1987, Publ. ASTM International, 1989, p. 266.
5. J.L. Lee and Y.T. Pan, Metall. Trans. A, vol.24A, 1993, p.1399.
6. H. Mabuchi and T. Ohashi, Proc. Int. Coll. "Hochleistungsstahlwerkstoffe", Freiberg, (Germany), 20-21 June 1996, Publ. TU Bergakademie Freiberg, 1996, p.35.
7. J. Takamura and S. Mizoguchi, Proc. "6th Int. Iron and Steel Congress", Nagoya (Japan), 1990, Publ. ISIJ, 1990, p.591.
8. C. van der Eijk, Ø. Grong, S. S. Babu, and S. A. David, Proc. "5th Int. Conf. on Trends in Welding Research", Georgia (USA), June 1-5, 1998, Publ. ASM International, 1999, p.729.
9. S. Ogibayashi, K. Yamaguchi, M. Hirai, H. Goto, H. Yamaguchi and K. Tanaka, Proc. "6th Int. Iron and Steel Congress", Nagoya (Japan), 1990, Publ. ISIJ, 1990, p.612.
10. R.C. Cochrane and D.J.Senogles, Proc. Conf. "Titanium Technology in Microalloyed Steels", Sheffield, UK, December 1994, Publ. The Institute of Materials, 1997, p.207.

11. A. O. Kluken and Ø. Grong, Metall. Trans. A, vol.20A, 1989, p.1335.
12. S.S, Babu, S.A. David, J.M. Vitek, K. Mundra and T. DebRoy, Mater. Sci. Technol., vol. 11, 1995, p.186.
13. A.G. Fox and D.G. Brothers, Scripta Metall., vol. 32, (7), 1995, p.1061.
14 K.W. Lange, Int. Mater. Rev., vol.33, (2), 1988, p.53.
15. N. Bannenberg, B. Bergmann and H. Gaye, Steel Research, vol.63, (10), 1992, p.431.
16. R.W.K. Honeycombe and H.K.D.H. Bhadeshia, Steels-Microstructure and Properties, London, Edward Arnold (Publishers) Ltd, 1995.
17. G.E. Dieter, Mechanical Metallurgy, 3rd ed., New York, McGraw-Hill, 1986.
18. H.K.D.H. Bhadeshia, Bainite in Steels, London, The Institute of Materials, 1992.
19. Ø. Grong and D. K. Matlock, Int. Met. Rev., vol.31, 1986, p.27.
20. Ø. Grong, Metallurgical Modelling of Welding, 2ed ed., The Institute of Materials, London, 1997.
21. Y. Ito, N. Masumitsu, and K. Matsubara, Trans. ISIJ, vol.21, 1981, p.477.
22. B. Sundman, B. Jansson, and J.-O. Andersson, CALPHAD, vol.9, 1985, p.153.
23. K.C. Hsieh, S.S. Babu, J.M. Vitek and S.A. David, Mat. Sci. and Eng., vol.A215, 1996, p.84.
24. C. van der Eijk, Ø. Grong and J. Walmsley, Mat. Sci. Techn., vol.16, 2000, p.55.

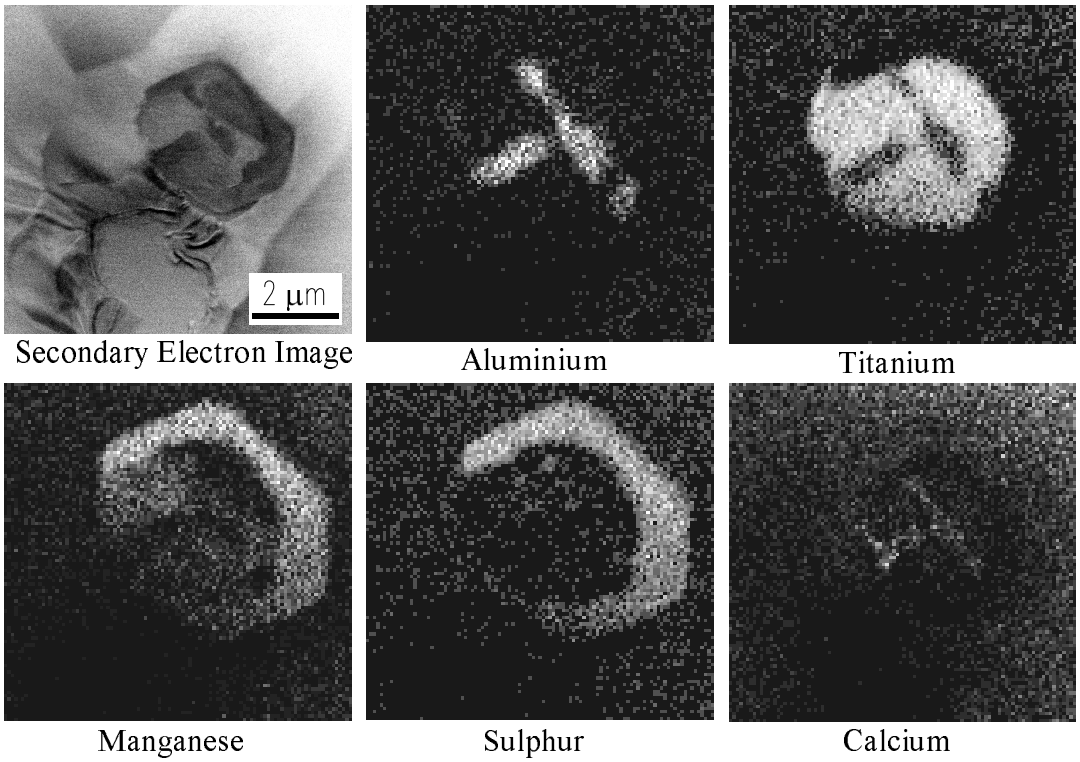

Figure 1: STEM X-Ray maps showing the element distribution in an inclusion from steel A

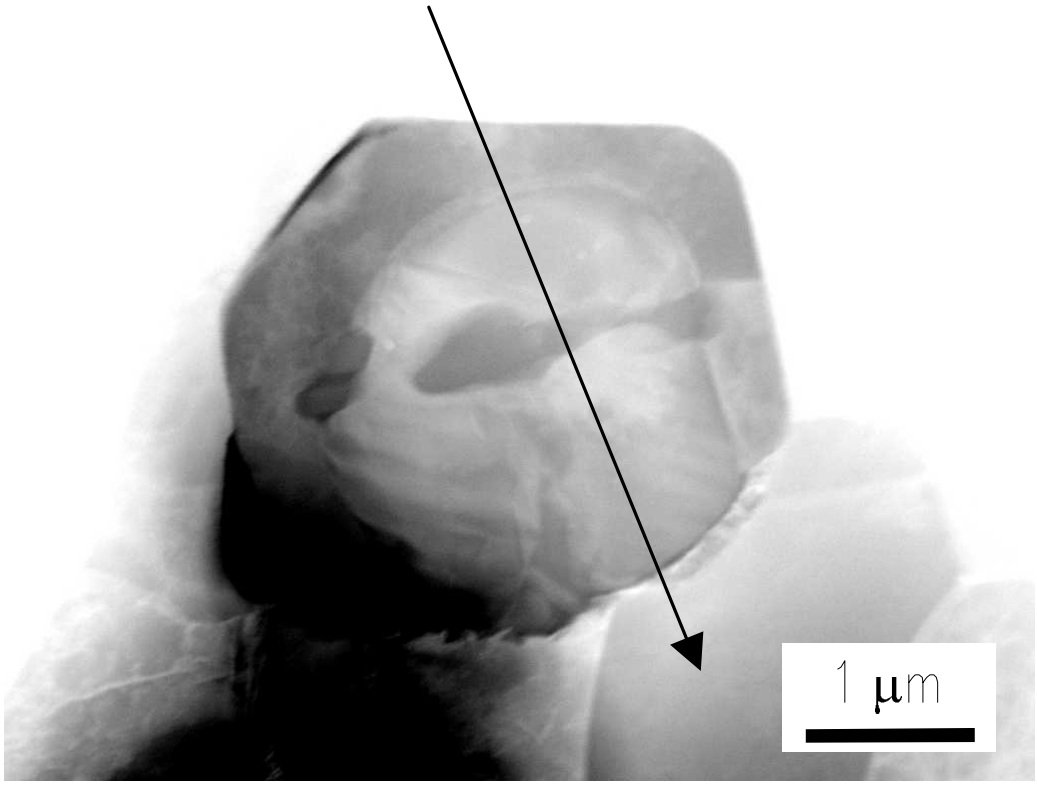

Figure 2: TEM bright field image of an inclusion in steel A. The arrow indicates where the linescan is taken across the inclusion

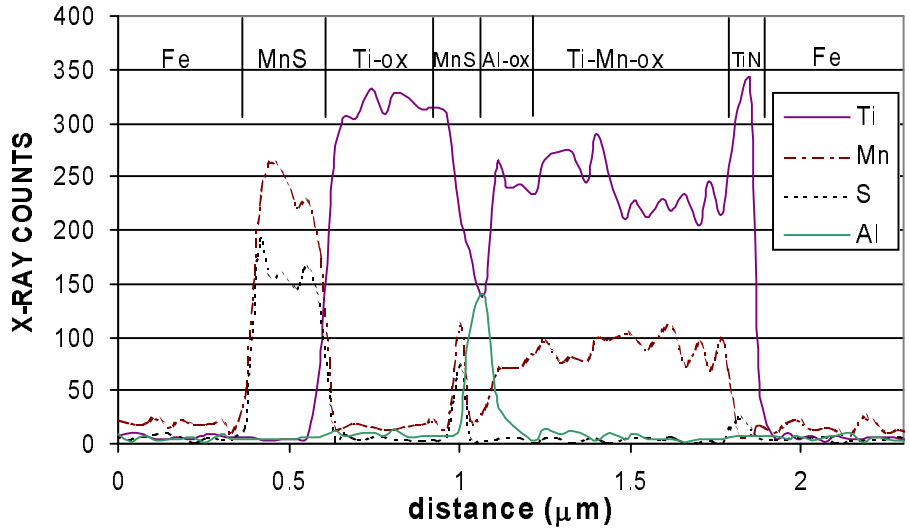

(a)

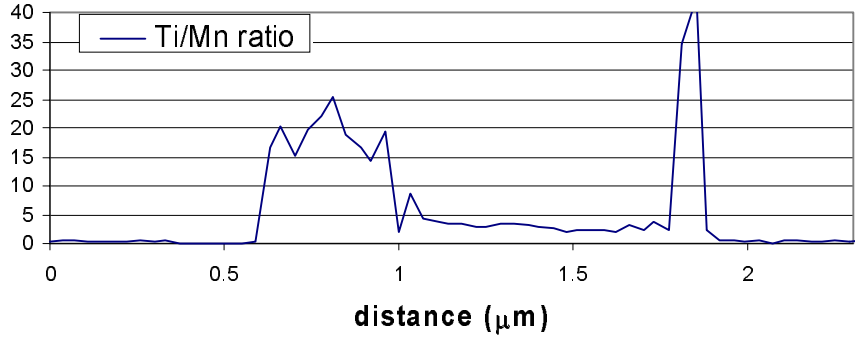

(b)

Figure 3: Summary of the results from the linescan across the inclusion in Figure 2; (a) X-ray counts of different elements, (b) Ratio between the Ti and the Mn X-ray counts

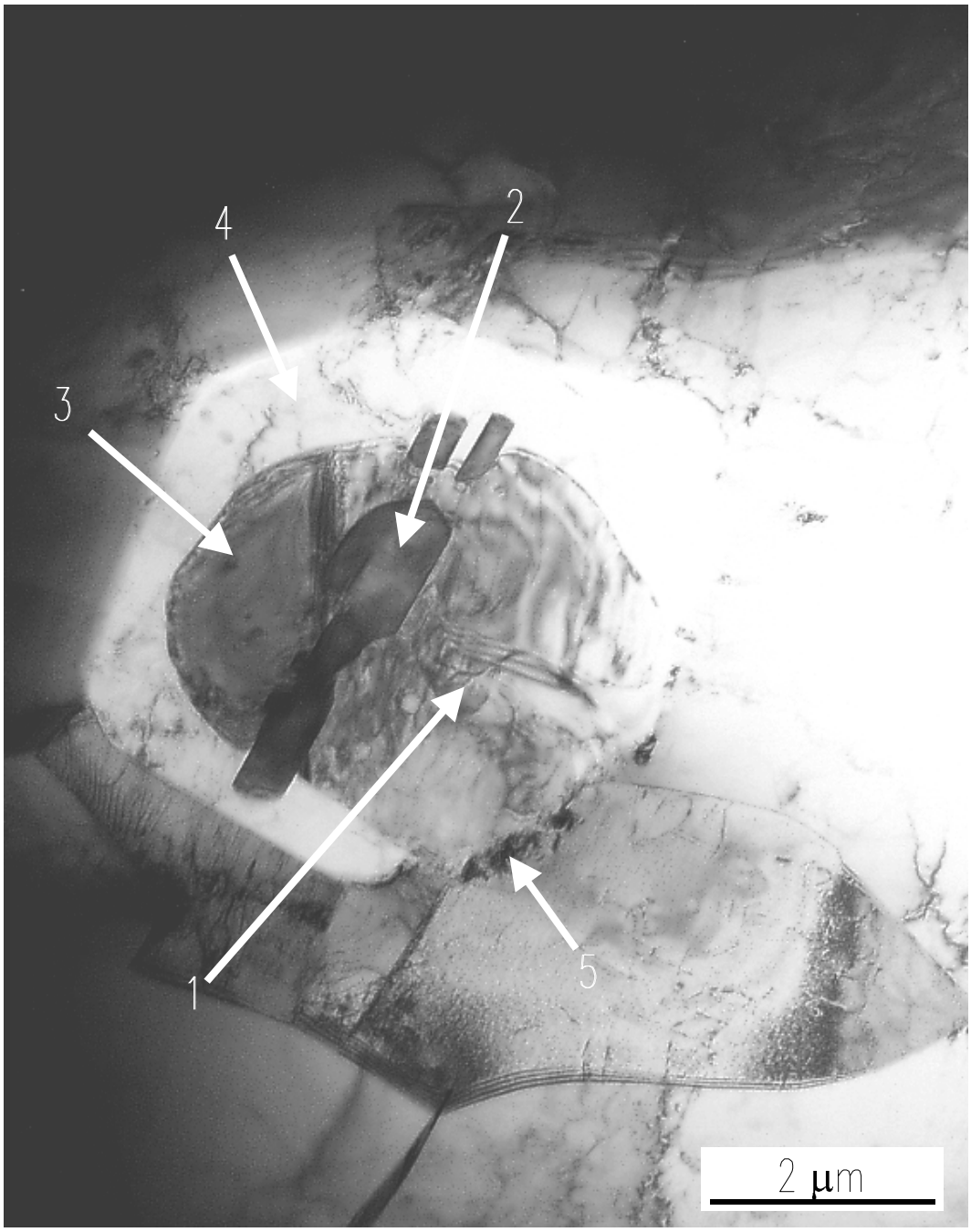

Figure 4: TEM bright-field image of an inclusion in steel A. The arrows indicate the location of the different phases

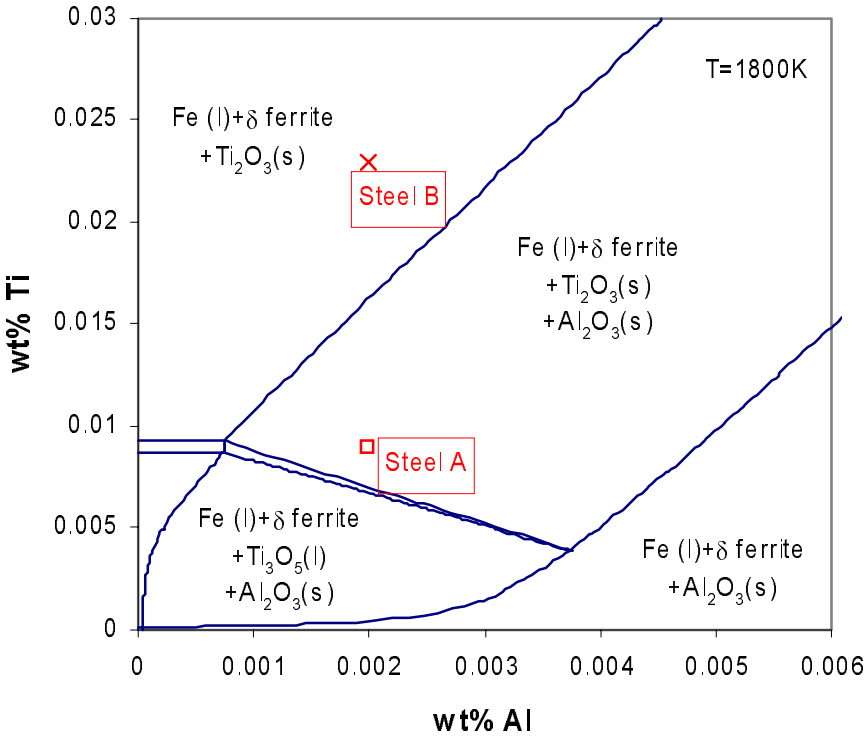

Figure 5: Oxides in equilibrium with steel containing 0.003wt%O at 1800K

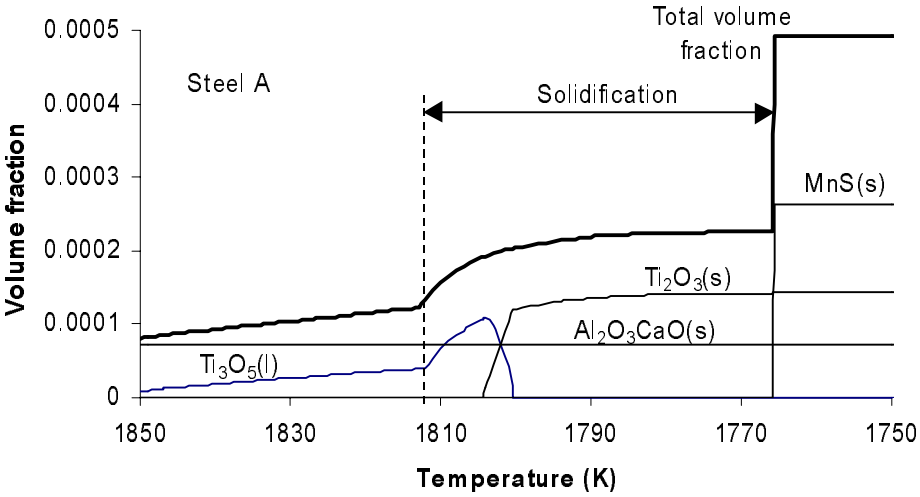
Steel A
Solidification
Total volume fraction
MnS(s)
Ti_2O_3(s)
Al_2O_3CaO(s)
Ti_3O_5(l)
Volume fraction
0.0005
0.0004
0.0003
0.0002
0.0001
0
1850
1830
1810
1790
1770
1750
Temperature (K)

(a)

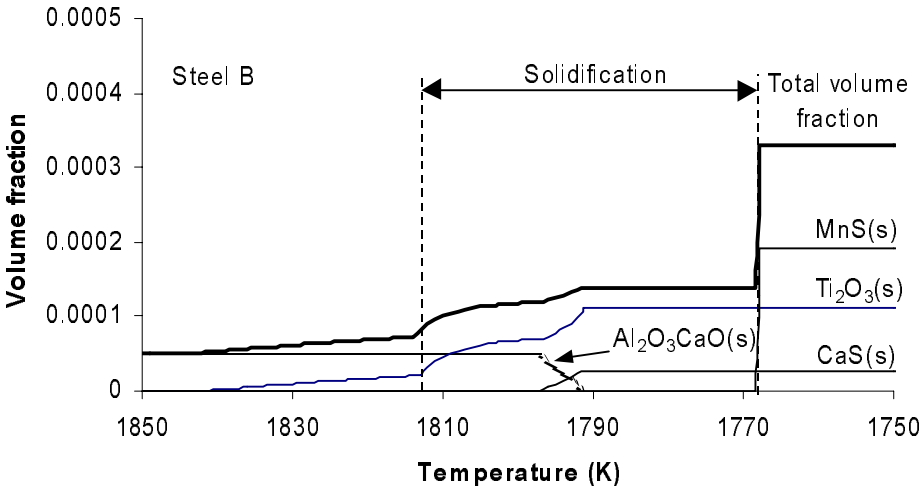
Steel B
Solidification
Total volume fraction
MnS(s)
Ti_2O_3(s)
Al_2O_3CaO(s)
CaS(s)
Volume fraction
0.0005
0.0004
0.0003
0.0002
0.0001
0
1850
1830
1810
1790
1770
1750
Temperature (K)

(b)

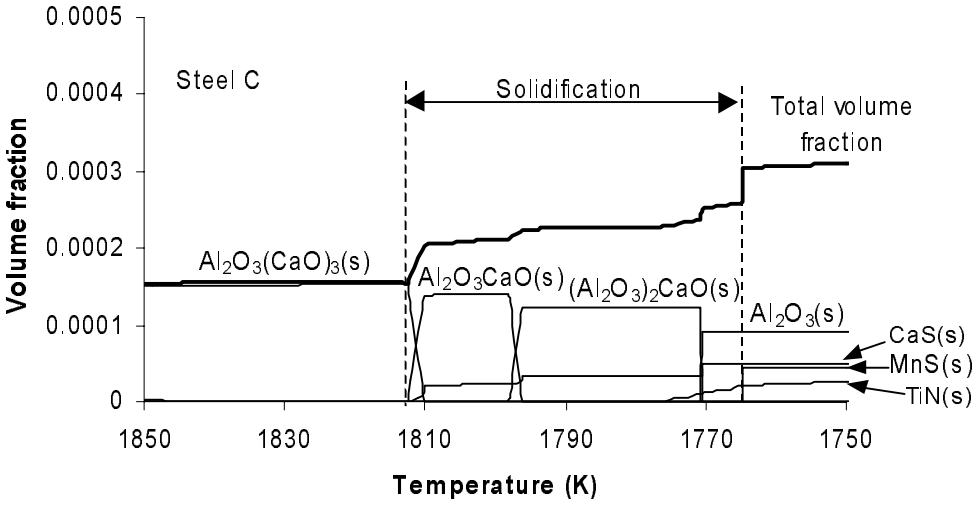

(c)

Figure 6: Summary of the results from the Thermo-Calc predictions based on the global equilibrium approach; (a) Steel A, (b) Steel B, (c) Steel C

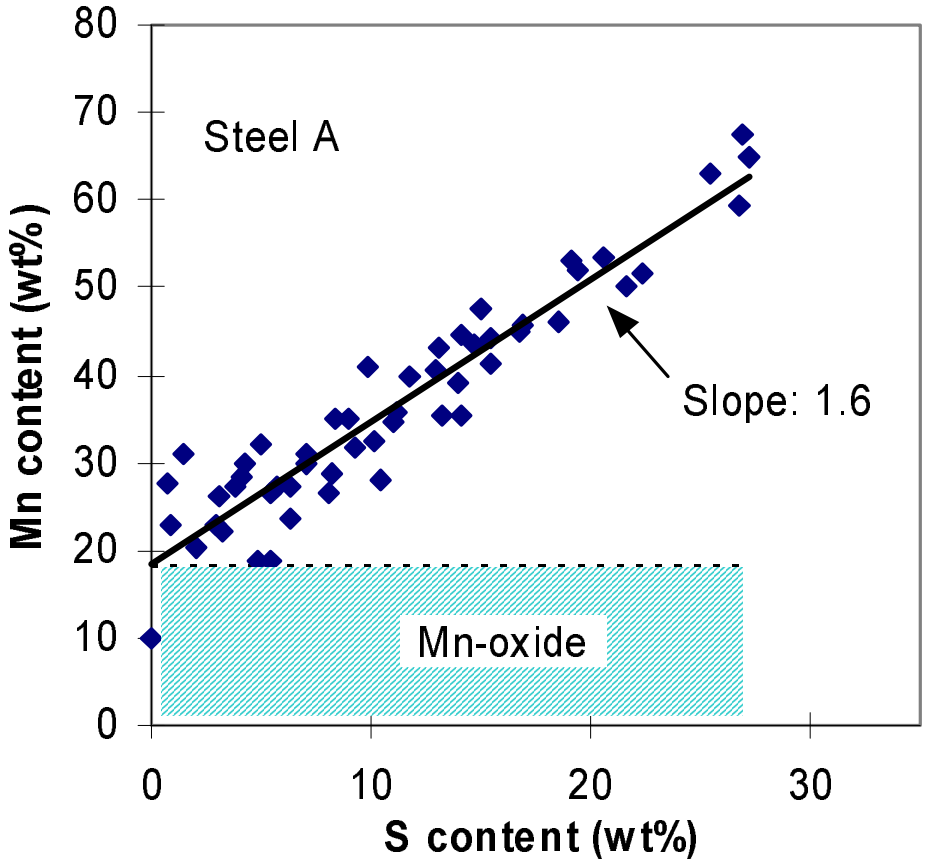
Steel A
Slope: 1.6
Mn-oxide
Mn content (wt%)
S content (wt%)
0
10
20
30
40
50
60
70
80
0
10
20
30

(a)

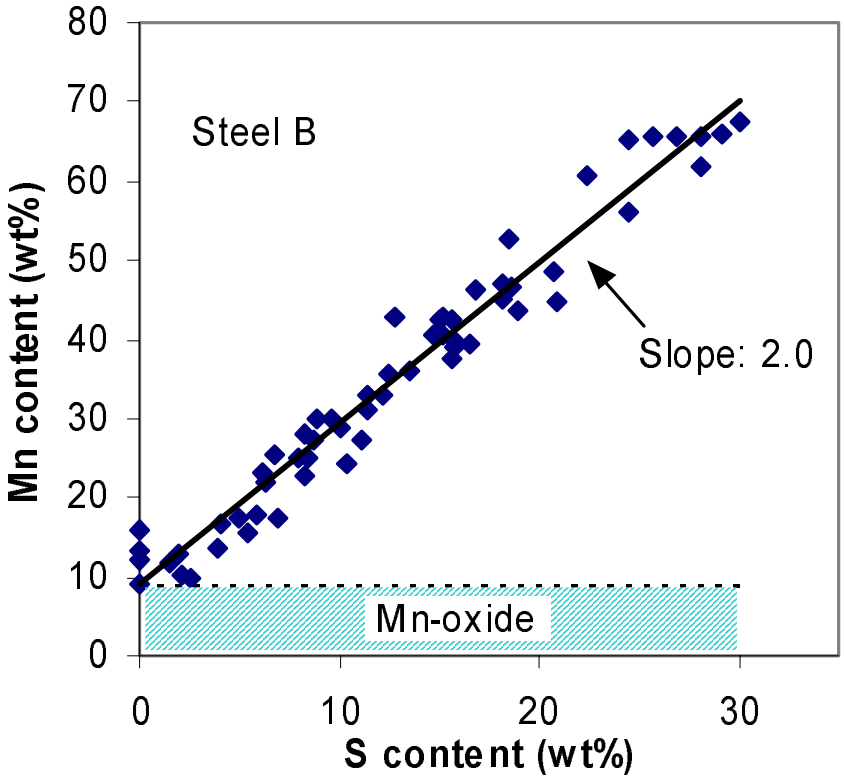

(b)

Figure 7: Plots showing the relationship between the measured Mn and S contents in the inclusions; (a) Steel A, (b) Steel B

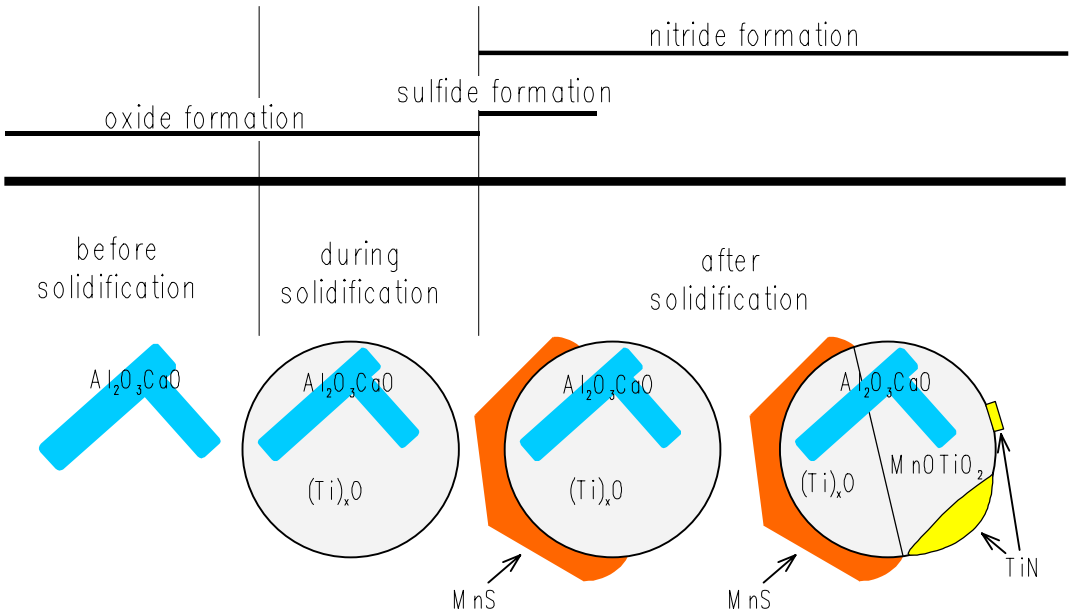

Figure 8: Schematic representation of the sequence of inclusion formation in Ti-deoxidised steels

Table I: Product analyses taken from the slab, quarter thickness position (wt%)

Steel	C	Si	Mn	S	Al	N	O	Ti	Ca
A	0.08	0.08	1.55	0.005	0.002	0.003	0.004	0.009	0.0007
B	0.06	0.09	1.40	0.004	0.002	0.002	0.002	0.023	0.0005
C	0.07	0.11	1.50	0.003	0.037	0.004	0.002	0.010	0.0027

Table II: Composition of oxysulphides observed in the steels A

	Steel A	Steel B	Steel C
Ti	29.4±14.1	45.7±22.1	1.6±2.6
Al	17.6±13.1	3.5±6.6	23.3±13.4
Mn	35.9±12.6	34.6±16.9	12.4±11.1
S	10.7±7.3	12.7±8.2	23.4±10.2
Ca	3.8±3.1	1.9±2.2	27.8±13.3
Mg	1.5±1.9	1.3±3.3	11.5±6.9
Si	0.9±0.8	0.2±0.5	0.1±0.4

Table III: Comparison between calculated and analysed inclusion compositions (wt%), based on outputs from Thermo-Calc at 1760K and raw data from Table II

Steel	A		B		C	
	analysed	calculated	analysed	calculated	analysed	calculated
Ti	29	26	46	29	2	10
Al	18	6	4	0	23	23
Mn	36	41	35	41	12	13
S	11	24	13	27	23	28
Ca	4	3	2	3	28	26
Mg	2	0	1	0	12	0
Si	1	0	0	0	0	0

Table IV: Comparison between calculated and analysed oxide core compositions (in wt%) after correcting for the MnS contribution. Experimental conditions as in Table III

Steel	A		B	
	analysed	calculated	analysed	calculated
Ti	41	74	70	100
Al	25	17	6	0
Mn	24	0	20	0
S	0	0	0	0
Ca	6	9	3	0
Mg	3	0	1	0
Si	1	0	0	0